Bioactive Materials 33 (2024) 100–113

Contents lists available at ScienceDirect

Bioactive Materials

journal homepage: www.keaipublishing.com/en/journals/bioactive-materials

Advancing neural regeneration via adaptable hydrogels: Enriched with Mg^{2+} and silk fibroin to facilitate endogenous cell infiltration and macrophage polarization

Yisheng Gao [a,1], Yingyu Wang [b,1], Jianye Zhang [a], Miao Zhang [a], Chaolun Dai [c], Yang Zhang [d,e], Luzhong Zhang [a], Liming Bian [d,e,f,g,**], Yumin Yang [a,*], Kunyu Zhang [d,e,f,g,***], Yahong Zhao [a,****]

[a] Key Laboratory of Neuroregeneration of Jiangsu and Ministry of Education, Co-innovation Center of Neuroregeneration, NMPA Key Laboratory for Research and Evaluation of Tissue Engineering Technology Products, Nantong University, Nantong, 226001, PR China
[b] Department of Physics and Astronomy, School of Natural Science, The University of Manchester, Manchester, M13 9PL, UK
[c] Medical School, Nantong University, Nantong, 226001, PR China
[d] School of Biomedical Sciences and Engineering, South China University of Technology, Guangzhou International Campus, Guangzhou, 511442, PR China
[e] National Engineering Research Center for Tissue Restoration and Reconstruction, South China University of Technology, Guangzhou, 510006, PR China
[f] Guangdong Provincial Key Laboratory of Biomedical Engineering, South China University of Technology, Guangzhou, 510006, PR China
[g] Key Laboratory of Biomedical Materials and Engineering of the Ministry of Education, South China University of Technology, Guangzhou, 510006, PR China

ARTICLE INFO

Keywords:
Adaptable hydrogels
Magnesium
Cell infiltration
Regenerative microenvironment
Peripheral nerve repair

ABSTRACT

Peripheral nerve injury is a complex and challenging medical condition due to the limited ability of nerves to regenerate, resulting in the loss of both sensory and motor function. Hydrogels have emerged as a promising biomaterial for promoting peripheral nerve regeneration, while conventional hydrogels are generally unable to support endogenous cell infiltration due to limited network dynamics, thereby compromising the therapeutic outcomes. Herein, we present a cell adaptable hydrogel containing a tissue-mimetic silk fibroin network and a dynamically crosslinked bisphosphonated-alginate network. The dynamic network of this hydrogel can respond to cell-generated forces to undergo the cell-mediated reorganization, thereby effectively facilitating the rapid infiltration of Schwann cells and macrophages, as well as the ingrowth of axons. We further show that the magnesium ions released from the hydrogel not only promote neurite outgrowth but also regulate the polarization of macrophages in a sequential manner, contributing to the formation of a regenerative microenvironment. Therefore, this hydrogel effectively prevents muscle atrophy and promotes the regeneration and functional recovery of nerve defects of up to 10 mm within 8 weeks. The findings from this study demonstrate that adaptable hydrogels are promising inductive biomaterials for enhancing the therapeutic outcomes of peripheral nerve injury treatments.

Peer review under responsibility of KeAi Communications Co., Ltd.

* Corresponding author. Key Laboratory of Neuroregeneration of Jiangsu and Ministry of Education, Co-innovation Center of Neuroregeneration, NMPA Key Laboratory for Research and Evaluation of Tissue Engineering Technology Products, Nantong University, Nantong, 226001, PR China
** Corresponding author. School of Biomedical Sciences and Engineering, South China University of Technology, Guangzhou International Campus, Guangzhou, 511442, PR China.
*** Corresponding author. School of Biomedical Sciences and Engineering, South China University of Technology, Guangzhou International Campus, Guangzhou, 511442, PR China.
**** Corresponding author. Key Laboratory of Neuroregeneration of Jiangsu and Ministry of Education, Co-innovation Center of Neuroregeneration, NMPA Key Laboratory for Research and Evaluation of Tissue Engineering Technology Products, Nantong University, Nantong, 226001, PR China
E-mail addresses: bianlm@scut.edu.cn (L. Bian), yangym@ntu.edu.cn (Y. Yang), kyuzhang@scut.edu.cn (K. Zhang), zhaoyh108@ntu.edu.cn (Y. Zhao).
[1] YG and YW contributed equally to this work.

https://doi.org/10.1016/j.bioactmat.2023.10.026
Received 24 July 2023; Received in revised form 24 October 2023; Accepted 24 October 2023

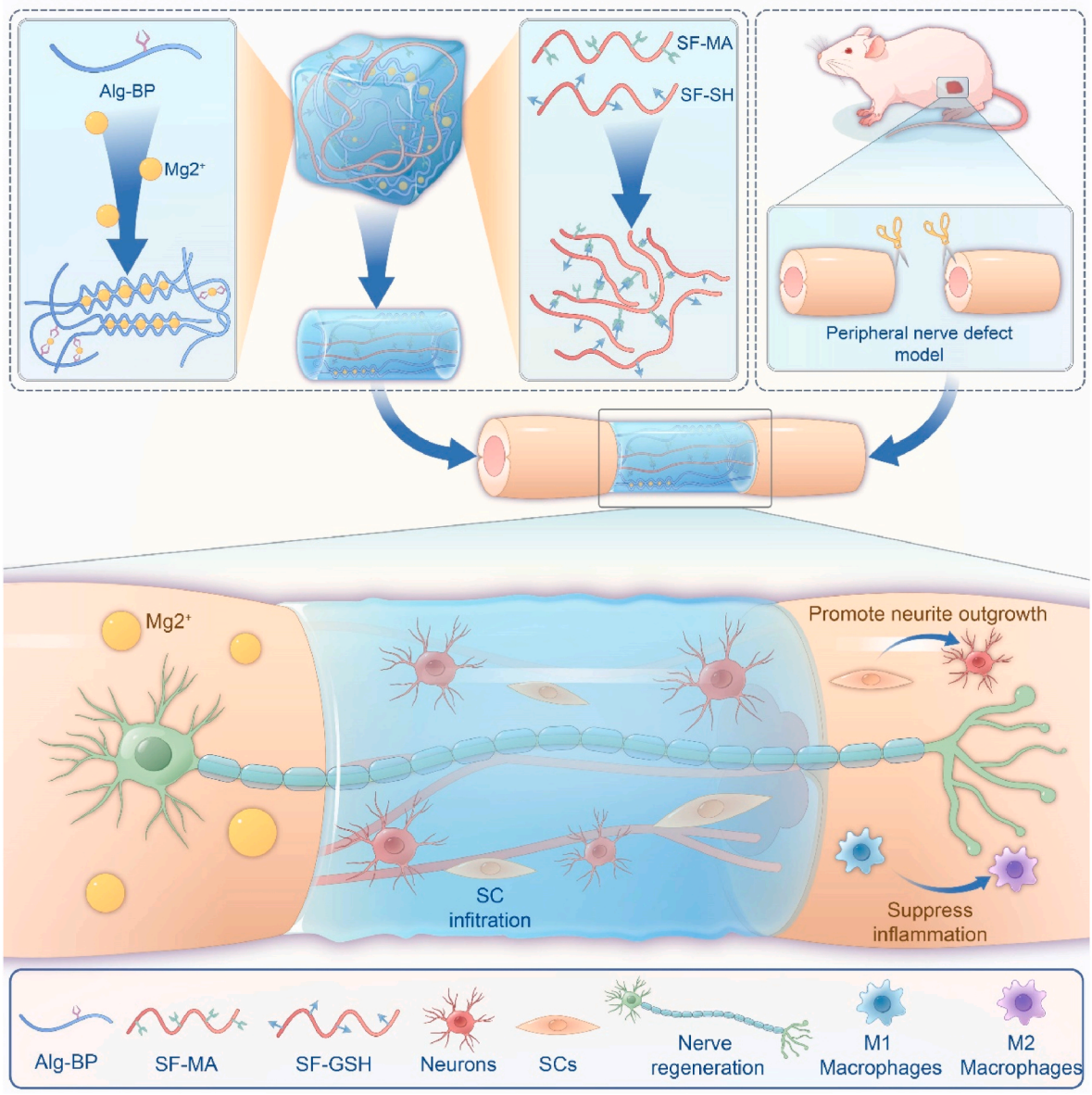

Fig. 1. Schematic illustration of the production of the Alg-Mg/SF adaptable hydrogel and its application in promoting peripheral nerve regeneration. The Alg-Mg/SF adaptable hydrogel consists of interpenetrating polymeric networks with Alg-Mg and SF. The hydrogel conduits can promote in situ peripheral never regeneration by facilitating the outgrowth of axons, infiltration of SCs, and recruit of macrophages.

1. Introduction

Peripheral nerve injury (PNI), frequently caused by trauma and tumor dissection, emerges as a profound clinical concern with far-reaching consequences, including loss of motor function and sensory perception [1,2]. Despite the relatively easier axon regeneration in the peripheral nerve system compared to the central nerve system, restoring damaged peripheral nerves in humans, particularly for long-distance nerve defects, remains a challenging task [3]. Such incomplete regeneration often results in functional disability of the patients and severely impacts their quality of life [4]. While autologous nerve grafting stands as the gold standard for the clinical therapy of PNI, it confronts a series of hurdles and risks, such as limited donor tissue availability, loss of sensitivity in the distribution area, and potential neuroma formation [5,6]. Consequently, it is of profound significance and substantial interest in developing alternative approaches for nerve regeneration and functional recovery after PNI using tissue engineering strategies.

The microenvironment governing peripheral nerve regeneration is a dynamic landscape of both biochemical and biophysical cues, regulating tissue regrowth and cell behaviors [7]. After PNI, macrophages, the initial immune cells to appear at the site of injury, assume a pivotal role in shaping the microenvironment essential for nerve regeneration [8,9]. Macrophages can polarize into either a pro-inflammatory M1 phenotype or a pro-healing M2 phenotype, and this is influenced by various stimuli within their microenvironment [10,11]. In addition, effective regeneration of peripheral nerve tissue necessitates the migration and maturation of Schwann cells (SCs) and the outgrowth of neurites, critical elements in nerve bridging [12]. Several studies have highlighted the potential application of magnesium ions (Mg^{2+}) in nerve regeneration, as it promotes macrophage polarization towards the M2 phenotype and enhances neurite outgrowth [13–15]. Oral administration of Mg^{2+} has been reported to enhance peripheral nerve regeneration after crush injury [16]. However, although magnesium and its alloy have been widely used as orthopedic implants, the delivery and application of Mg^{2+} in neural tissue engineering remain challenging. Moreover, silk fibroin (SF), a fibrous protein derived from the cocoons of domestic

silkworm *Bombyx mori*, exhibits remarkable biocompatibility and low immunogenicity, thus emerging as a promising biomaterial for neural regeneration [17]. Its filamentous microstructure and binding sites offer essential support for the infiltration and adhesion of SCs and neurons.

While biochemical signals have garnered substantial attention, the role of mechanical stimulation, equally crucial for nerve system development and function maintenance, has been comparatively less explored [18–20]. However, PNI damages the local mechanical niche due to the peripheral connective tissues and extracellular matrix (ECM) destruction. Inspired by the dynamic nature of natural ECM, cell-adaptable hydrogels emerge as a viable solution, responding to cell-generated forces and permitting cell-mediated remodeling of the matrix [21]. These features establish a suitable microenvironment, specifically a mechano-microenvironment, fostering multiple cellular activities, and demonstrating enhanced viability, proliferation, migration, differentiation, and paracrine effects of various cell types [22]. Cell-adaptable hydrogels can be fabricated from diverse natural or synthetic polymers, such as collagen, alginate, hyaluronic acid or polyethylene glycol, crosslinked via reversible interactions such as host−guest interactions, ionic interactions, and hydrogen bonding [23]. The dynamic hydrogel network, thus formed, responds to cell-generated forces, facilitating cell-mediated reorganization, and effectively supporting the rapid infiltration and mechanosensing of endogenous cells. Although cell-adaptable hydrogels have proven effective in promoting tissue repair, such as cartilage, bone and skin regeneration [24], their use in nerve repair remains limited.

In the present study, we investigated the potential of adaptable hydrogels to promote peripheral nerve repair by reconstructing the regenerative microenvironment (Fig. 1). Leveraging both biochemical cues (i.e., Mg^{2+} and SF) and biomechanical cues (i.e., network dynamics), we engineered nerve conduits using adaptable hydrogels. Owing to highly dynamic interactions between bisphosphonate-modified alginate (Alg-BP) and Mg^{2+}, the obtained hydrogels exhibited remarkable dynamic properties, and the thiol-ene click reaction between glutathione (GSH) and methacryloyl (MA) groups on SF created the interpenetrating polymer network (IPN). To evaluate the performance of the cell-adaptable Alg-Mg/SF hydrogel, we implanted it into a 10-mm nerve defect in vivo. The adaptable hydrogels facilitated favorable cell-material interactions, including SCs migration and neurite outgrowth, contributing to muscle recovery from atrophy and nerve functional recovery. We next investigated the mechanism underlying the enhanced nerve regeneration induced by Alg-Mg/SF hydrogels and found that such hydrogels could rapidly recruit macrophages in the short term and then promoted their M2 transition. Overall, this study demonstrates the potential of adaptable hydrogels as a promising new approach for the treatment of peripheral nerve injuries, leading to improved functional outcomes.

2. Methods

2.1. Primary DRG neuron culture

Dorsal root ganglion (DRG) was isolated from embryonic (E14) Sprague-Dawley rats. DRGs were pulled off with micro-forceps and transferred to 1 × PBS, where the axon roots and dural tissues were manually removed. DRGs were seeded into 6 culture dishes containing Neurobasal medium (Gibco, USA) in supplement with B27 (Thermo Fisher, USA), glutamine (Gibco, USA), and NGF (20 ng/ml; Sigma Aldrich, USA). Different concentrations of Mg^{2+} (0, 10, 20, 40, 80, and 160 mM) were added into the medium the next day, and the DRGs were cultured for another 24 h prior to fixation with 4 % paraformaldehyde. The cells were stained with anti-neurofilament 200 antibody (1:600 dilution; Sigma, USA) and then Alexa Fluor 488 secondary antibody (1:600 dilution; Abcam, USA). Fluorescent images were acquired using a fluorescent microscope epifluorescence microscope (ZEISS, Imager.M2, Germany).

DRG neurons were removed from the embryonic (E14) Sprague-Dawley rats, and transferred to fresh HBSS medium, where the axon roots and dural tissue were manually removed. The DRG neurons were then transferred to 0.1 % collagenase type I. Following 30 min incubation at 37 °C, the DRG neurons were dissociated in 0.25 % trypsin (Gibco) for an additional 10 min at 37 °C, and mechanically triturated through a pipette into the single cell suspension.

2.2. Synthesis of bisphosphonated-alginate (Alg-BP)

Alginate (tissue engineering grade) with ultra-low heat source was purchased from Mingyue Co., Ltd. (Qingdao, Shandong, China). Pamidronate disodium (410.28 mg) was dissolved in MES buffer (8 ml, pH = 7.0). Then, Alg (100 mg) was added into the above solution, followed by the addition of N-hydroxysuccinimide (NHS) (137 mg). Next, 1-(3-dimethylaminopropyl)-3-ethylcarbodiimide hydrochloride (EDC) (241.92 mg) was dissolved in MES buffer (2 ml, pH = 7.0) and added into the mixture dropwise with continuously stirring. The reaction was proceeded for 24 h at room temperature. Thereafter, the reaction mixture was transferred into a dialysis membrane with Mw cutoff of 3.5 kDa and dialyzed against NaCl gradient solution and then deionized water for 3 days, frozen at −80 °C, lyophilized and stored at −20 °C in powder form. The incorporation of bisphosphonate group was verified by ^1H NMR in D_2O.

2.3. Preparation of silk fibroin stock solution

Silk fibroin was degummed in 0.5 % Na_2CO_3 solution for 30 min and repeated for three times, then disposed into a ternary solvent system of $CaCl_2/C_2H_5OH/H_2O$ (molar ratio = 1:2:8) at 75 ± 2 °C. The solution was dialyzed in deionized water for 72 h. To synthesize the glutathione (GSH) modified SF (SF-GSH), the carboxyl groups on SF were activated by EDC/NHS (0.5 mg/mL of EDC with 0.7 mg/mL of NHS in PBS buffer) for 20 min at room temperature. Then, GSH was added to a final concentration of 2 g/L into the above mixture. The reaction is carried out for 1 h at room temperature, and the unreacted GSH in the solution were removed by dialysis for 3 days at 4 °C [25]. The degree of GSH coupling was determined using a reduced glutathione colorimetric assay kit (Elabscience, E-BC-K030-M) according to manufacturer's protocol. To gain the highly concentrated SF-GSH solution, the aqueous SF-GSH solution was subjected to airflow at 4 °C to evaporate the water and prevent the SF-GSH from self-crosslinking. The SF methacryloyl (SF-MA) was purchased from Yongqinquan (China) and dissolved in DI water at 10 mg/ml.

2.4. Preparation of the Alg/SF IPN hydrogels and nerve conduits

Alg-BP was dissolved in HEPES buffer (pH = 7.4), followed by mixing with the concentrated solution of SF-GSH and SF-MA. The hydrogels were cast by rapidly mixing the Alg-BP/SF solution with a $CaSO_4$ or $MgCl_2$ slurry via two syringes and ejecting the mixture between two glass plates, where it gelled over 1.5 h. Four different hydrogels were designed, i.e., Alg hydrogel, Alg-Mg hydrogel, Alg/SF hydrogel, and Alg-Mg/SF hydrogel, respectively (Table S1). The stainless-mold was employed to generate nerve conduits.

2.5. Mechanical properties of hydrogels

The rheological test was carried out by a HAAKE MARS rheometer (Thermo Scientific). The storage (G') and loss (G'') moduli of the hydrogels were measured under constant strain (1 %) and frequency (1 Hz). Meanwhile, to determine the linear viscoelastic range of the hydrogels, the frequency (10–0.1 Hz) sweeps were performed at 0.1 % constant shear strain. The suture and tensile strengths of 12 mm hydrogel conduits were assessed at a rate of 2 mm/min, employing the universal test machine (MTS) in tensile mode.

2.6. Swelling test

The initial mass of the hydrogels was recorded as W_0, and the hydrogels were submerged in PBS at 37 °C. At different preset time points, the mass of the specimens was weighed (W_1) after using filter paper to absorb the residual liquid on the surface of hydrogels. The following formula was applied to calculate the swelling rate:

$$SR = (W_1 - W_0) / W_0 \times 100\%$$

2.7. SEM characterization

The microscopic morphology of the cross-section of the hydrogel was observed by scanning electron microscopy. After being frozen by liquid nitrogen and lyophilized, the hydrogel specimens were cut in half, fixed on a stage, and sprayed with a thin layer of gold. Images were acquired at an accelerating voltage of 30 kV, and at least 50 pores in each sample were measured randomly to analyze the pore size of the hydrogels.

2.8. Hydrophilicity test

The hydrophilicity of hydrogel was characterized by contact angle measurement. After absorbing excess water on the surface, the hydrogel samples were placed on a flat measuring table. A single drop of distilled water was added onto the surface of the hydrogel, and the contact angle between water and the surface of the hydrogel was measured. At least 3 independent measurements were done for each sample.

2.9. Quantification of the release of magnesium ions from hydrogels

The Alg-Mg or Alg-Mg/SF hydrogels were immersed in HEPES buffer (pH = 7.4, containing 2 mM Ca^{2+}) under 37 °C. 100 μL of supernatant was collected at each preset time point followed by the addition of 100 μL of fresh buffer or solution. All samples were in triplicate (n = 3). The supernatant samples were analyzed by magnesium colorimetric assay kit (Nanjing Jiancheng) according to manufacturer's protocol.

2.10. Analysis of DRG neurons encapsulated in hydrogels

For 3D cell culture, DRG neuron cell suspension was mixed with the precursor solution of Alg/SF IPN hydrogels to reach a final concentration of 1×10^7 cells mL^{-1}. The mixture was quickly pipetted between two glass plates. Once the Alg/SF gelled in the plates within 0.5 h, small plugs (diameter = 8 mm; height = 2 mm) were punched out of the gels and placed in the wells of a 24-well plate. The obtained DRG neurons encapsulated in hydrogels were cultured in Neurobasal and B-27 (Gibco) supplemented with uridine (10 nM), FdUr (10 nM), penicillin–streptomycin (50 U/ml, Gibco), glutamine (2 mM) and NGF (50 ng/ml). After cultured for 3 days, the hydrogels were stained with anti-neurofilament 200 antibody (1:600 dilution; Sigma, USA) and then Alexa Fluor 488 secondary antibody (1:600 dilution; Abcam, USA), and imaged by a confocal microscopy (LSM 900, Ziss, Germany) with ZEN3.5 software (excitation/emission 488 nm/507 nm). Images at various depths were captured and a series of micrographs were later combined for "z-stacked'' compilation images.

2.11. Culture of primary SCs and fibroblasts

Primary SCs were collected from the sciatic nerves of 1-day old Sprague Dawley (SD) rats, digested with trypsin and collagenase and cultured with DMEM medium supplemented with 10 % fetal bovine serum (FBS). The SCs were then purified by anti-Thy 1.1 antibody and complement as described previously [26]. Primary cultures of SCs were maintained at 37 °C in DMEM containing 10 % FBS in a humidified environment containing 5 % CO_2.

The sciatic nerve of 3-day old Sprague Dawley (SD) rats were used to cultivate fibroblast cells, as described previously [27]. Briefly, the sciatic nerves were digested with 0.125 % trypsin for 30 min and 1 % collagenase for 10 min at 37 °C. The cells were cultured with DMEM medium supplemented with 10 % FBS. After 1 h, the supernatant was discarded and cultured with fresh DMEM medium supplemented with 10 % FBS. Subsequently, the medium was changed every two days with DMEM supplemented with 10 % FBS. The final preparations consisted of 98 % fibroblasts.

2.12. In vitro culture of SCs and RAW264.7 with hydrogel

RAW264.7 cells were cultured in DMEM supplemented with 10 % FBS,100 units/mL of penicillin, and 100 μg/mL of streptomycin. Primary SCs and RAW264.7 cells were seeded onto each hydrogel surface in the 96-well culture plate at a density of 5000 cells per well and incubated for 0.5 h and 2 h at 37 °C. The morphology of cells was observed by optical microscopy.

Live/dead cell staining was performed on day 1 and day 4 according to the manufacturer's protocol (Invitrogen, USA), where living cells are stained green with calcein-AM, and dead cells are stained red with propidium iodide. The stained cells were observed using a Leica fluorescent microscopy. For the 3D encapsulation of SCs, once the primary SCs reach a density of 70%–80 %, they were detached from the culture dish using 0.25 % trypsin digestion and collected into centrifuge tubes. These cells were then pelletized via centrifugation. Next, 3 % Alg-BP solution dissolved in HEPES solution was gently mixed with SCs using a pipette, and the mixture was further combined with specific concentrations of magnesium sulfate, calcium sulfate, and SF to create the Alg-Mg/SF hydrogels that encapsulated SCs.

2.13. Analysis of SCs infiltration in the hydrogels in vitro

The migration test was performed by using a 24-well transwell. The Alg, Alg-Mg, Alg/SF, and Alg-Mg/SF hydrogels were formed on the top of the transwell membrane, respectively. Then, the transwell setups were placed in a 24-well plate. The volume of each hydrogel was 100 μL. Next, 100 μL of media containing SCs (1×10^5/mL) were added to the top of the hydrogels, and 750 μL of growth media with 50 ng/ml NGF were added to the 24-well plates. After 2 h and 3 days of incubation at 37 °C, the hydrogels were fixed with 4 % paraformaldehyde and stained with DAPI. Confocal micrographs were obtained to visualize the distribution of the cells in the hydrogels.

2.14. Quantitative real-time PCR (qRT-PCR)

Total RNA was extracted from cells using Trizol reagent (Invitrogen) and subsequently transcribed into cDNA utilizing a cDNA synthesis kit (Takara). Gene expression analysis was conducted using the StepOne Real-Time PCR Detection System (Applied Biosystems) with SYBR Green Supermix. The mRNA levels were normalized to GAPDH, which served as a housekeeping gene. The primer sequences used were: GAPDH forward:5′-GGCTCTCTGCTCCTCCC-3′; GAPDH reverse: 5′-CCGTTCACACCGACCTT -3′; *BDNF* forward: 5′-TGACAGTATTAGCGAGTGGG-3′; *BDNF* reverse: 5′-GATTGGG TAGTTCGGCATT-3′; *NGF* forward: 5′-CCTCTTCGGACACTCTGG-3′; *NGF* reverse: 5′-CTCCAACCCACACACTGA-3′; *Arg-1* forward: 5′-CTGGGGATTGGCAAGGTGAT-3′; *Arg-1* reverse: 5′-CCTGAAAGGAGCCCTGTCTT-3′; *TGF-β1* forward: 5′-ACTGGAGTTGTACGGCAGTG-3′; *TGF-β1* reverse: 5′-TCTTCTCTGTGGAGCGTTGA-3′; *RAB21* forward: 5′-ACCGAGATTCGAATGGAGCTA-3′; *RAB21* reverse: 5′-CCCACAGACTCTGCATACGATT-3′; *RTN3* forward: 5′-TGACTCCTTGAAGCTGGCTG-3′; *RTN3* reverse: 5′-CCGGGCAATCCCAACATAGT-3′.

2.15. Sciatic nerve transection and hydrogel implantation

The SD rats were approved by the Laboratory Animal Center of Nantong University and complied with institutional and international

guidelines (Approval ID: SYXK [SU] 2017-0046). A total of 95 adult male Sprague-Dawley rats (8–10 weeks old, weight range 180–200 g) were used as experimental animals (Table S2). The SD rats were anesthetized by intraperitoneal injection of 2 % sodium pentobarbital saline solution. The SD rats were anesthetized and underwent bridging surgery under aseptic conditions. The left hind leg of all rats was used as the experimental side, and the severed sciatic nerve was subjected to nerve graft bridging surgery. In the control group, a section of the sciatic nerve was excised leaving a 10 mm long defect after contraction of the nerve endings. In the experimental group, hydrogel conduits were connected to both ends of the sciatic nerve at the same defect distance, and a polycaprolactone was used to wrap the hydrogel for easy suture.

2.16. Immunofluorescence analysis of regenerated axons

At 1 week, 2 weeks, and 8 weeks post-surgery, regenerated nerves were dissected and harvested after perfusion of 4 % paraformaldehyde through the rat's circulatory system. A neonatal segment was selected from the proximal portion of the duct near the spine. Nerve grafts were harvested using a freezing microtome and cut transversely into 10 μm thick slices. The intermediate ductal section was selected and cut longitudinally into 10 μm thick sections using a frozen sectioning machine. Cryosections were incubated overnight at 4 °C with S100 (1:200; Rabbit monoclonal antibody, Abcam), NF200 (1:600; Mouse monoclonal antibody, Sigma), CD86 (1:400; Mouse monoclonal antibody, Abcam), CD68 (1:400; Rabbit monoclonal antibody, Abcam) and CD206 (1:400; Rabbit monoclonal antibody, Abcam) primary antibodies for immunofluorescence staining. Sections were then incubated with goat anti-mouse IgG Alexa Fluor 488 (1:600, Abcam) and Cy3-labeled goat anti-rabbit IgG (1:200; Abcam), respectively, at room temperature for 2 h each. Sections were washed with PBS. The NF/S100-immunoreactive signals at predetermined thresholds value were quantified, and the CD68, CD86, and CD206 positive cells were counted using ImageJ software [28].

2.17. TEM observation

At 8 weeks post-surgery, the sciatic nerve samples from the injured side were excised, trimmed, and fixed in a pre-cooled mixture of 0.5 % glutaraldehyde. After washing and dehydration, the tissues were embedded in Epon 812 epoxy resin, cut into 60-nm-thick sections, and stained with lead citrate and uranyl acetate. The stained sections were observed under TEM (Hitachi, Japan). The thicknesses of myelin sheaths, the diameters of myelinated fibers, and the number of myelin lamellae were quantified with ImageJ.

2.18. Wet weight and histologic assessment of gastrocnemius muscle

The gastrocnemius muscle was collected from the experimental and control sides for weighing at 8 weeks after surgery. First, the muscle wet weight ratio (%) was calculated: muscle wet weight of the experimental limb/weight of the contralateral control limb × 100 %. It was then fixed and embedded in paraffin and cut into cross-sections for Masson trichrome staining (ab150686, Abcam) and examined for pathological changes in the gastrocnemius muscle. The longitudinal sections of the gastrocnemius (10 μm) were also undergone overnight incubation with α-Bungarotoxin (BTX) conjugated to Alexa-555 (B35450, Invitrogen, USA) targeting neuromuscular junction (NMJ) at 4 °C to count the area of motor endplates. The motor endplates in 3 random fields with high magnification (× 200) per animal were calculated for area statistical analysis. Images were photographed under a fluorescent microscope epifluorescence microscope (ZEISS, Imager M2, Germany). The areas of muscle fibers and motor endplates were counted by ImageJ software [29–31].

2.19. Electrophysiological assessment

Electrophysiological analysis was performed after 8 weeks of bridging the sciatic nerve. The sciatic nerve on the experimental side was re-exposed under anesthesia. Grounding electrodes were fixed to the epidermis of the rats and recording electrodes were accurately implanted into the muscle belly of the gastrocnemius muscle. The proximal and distal sciatic nerves of the amputated segment were measured continuously to obtain compound muscle action potential (CMAP) and other data. CMAP peak amplitude values were recorded and compared across groups.

2.20. Walking track assessment

To characterize the functional recovery at 8 weeks after surgery, the rats were placed on the CatWalk XT (Noldus) apparatus and the footprints of each group were recorded separately. This experiment focused on comparing the sciatic function index (SFI) between groups at different time points post-operatively, with the following formula:

$$SFI = -38.3\left(\frac{EPL - NPL}{NPL}\right) + 109.5\left(\frac{ETS - NTS}{NTS}\right) + 13.3\left(\frac{EIT - NIT}{NIT}\right) - 8.8$$

(PL: the distance from the heel to the tip of the third toe. TS: the distance from the first toe to the fifth toe. IT: the distance from the second toe to the fourth toe. E: the experimental side. N: the normal side.)

2.21. RNA sequencing and bioinformatics analysis

We collected the regenerated nerves at proximal end at 1, 4 and 7 d following treatment with different samples for library construction and RNA-seq. Total RNA of each sample was quantified and qualified by Agilent 4150 Bioanalyzer (Agilent, USA) and NanoDrop (Thermo Fisher, USA). The qualified samples were used for library construction. 1 μg total RNA was used for following library preparation. Finally, the library preparations were sequenced on MGISEQ-T7 (MGI, China) and 150 bp paired-end reads were generated. The sequences were processed and analyzed by APTBIO, in which mRNAs with an absolute fold change (FC) ≥ 2 and p-value <0.05 were considered as differential expression were used for further downstream analysis. For statistical analysis, the unsupervised principal component analysis (PCA) was performed in R (v3.6.0) using standard k-means algorithms (Bayesian, Silhouette, Elbow) for finding optimal clusters, and mRNAs were clustered into groups based on expression levels by R 'hclust' function with the parameter of method = "ward.D". For enrichment analyses, gene ontology (GO) and KEGG pathways (Release 91.0) enrichment were performed with R "clusterProfiler" (3.14.3) package. Heatmaps were used to visualize the expression of genes across the samples.

2.22. Statistical analysis

All data are presented as the means ± standard deviations (SDs). Statistical differences were determined by performing a one-way factorial analysis of variance and Tukey's post hoc test. GraphPad Prism 8 (GraphPad Software) was used for statistical analysis. Tests were conducted with a 95 % confidence interval ($\alpha < 0.05$), and statistical significance was set at $p < 0.05$.

3. Results

3.1. Fabrication and characterization of the cell-adaptable Alg-Mg/SF hydrogel

To manufacture hydrogels, we first synthesized bisphosphonate (BP)-modified alginate (Alg) and glutathione (GSH) modified SF (SF-GSH) using carbodiimide chemistry. The activation of carboxyl groups

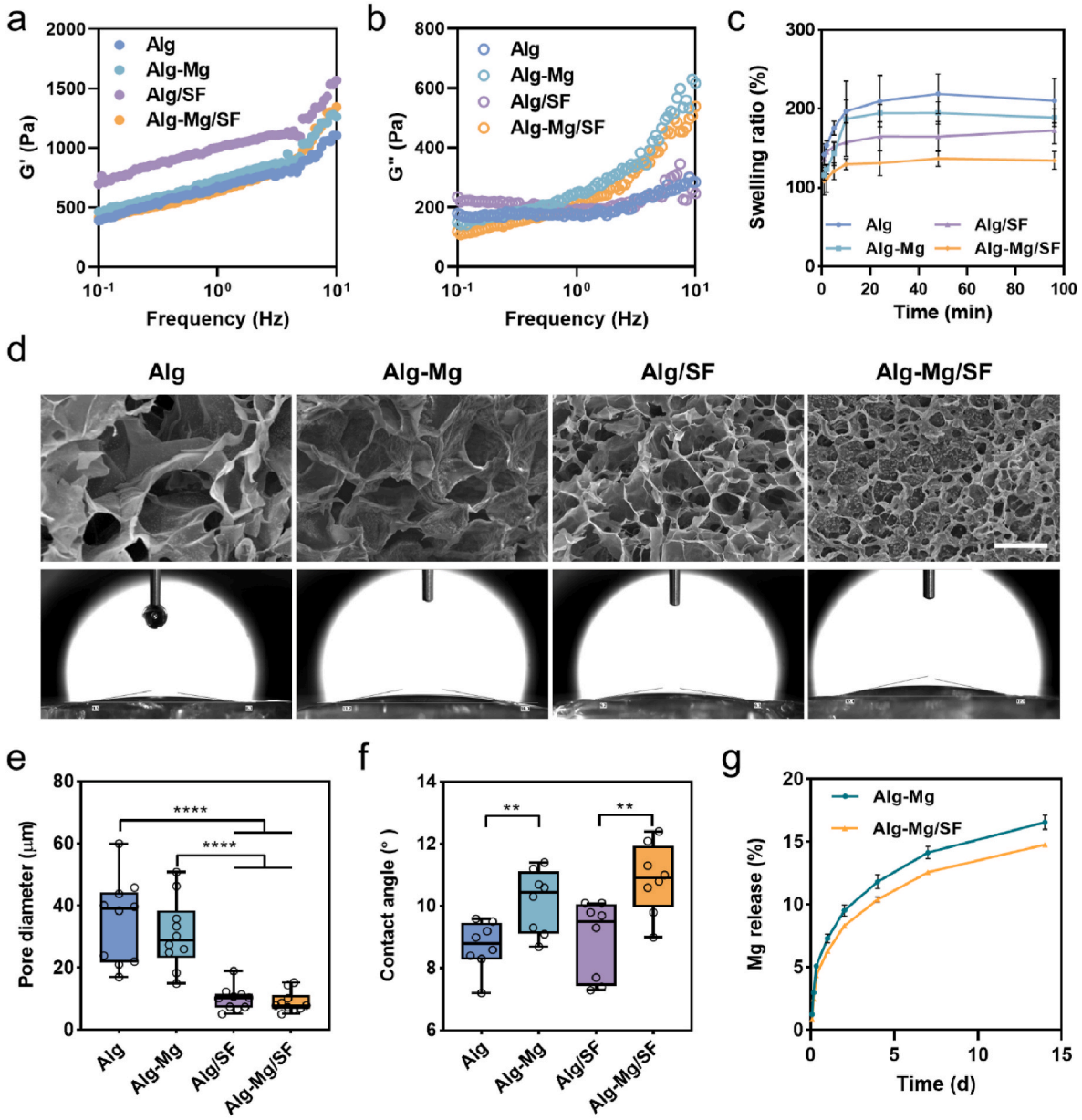

Fig. 2. Fabrication and characterization of the cell-adaptable Alg-Mg/SF hydrogel. (a) Storage modulus G′ and **(b)** loss modulus G″ as a function of frequency for the adaptable hydrogels. **(c)** Swelling kinetics of the Alg-Mg/SF hydrogel (n = 3). **(d)** SEM characterization and photographs of water contact angles of the Alg-Mg/SF hydrogel; scale bar = 50 μm. **(e)** Pore size analysis of the Alg-Mg/SF hydrogel (n = 10); $^{****}p < 0.0001$. **(f)** Water contact angles of the Alg-Mg/SF hydrogel (n = 8); $^{**}p < 0.01$. **(g)** Cumulative release profile of Mg^{2+} from the Alg-Mg/SF hydrogel in PBS over 14 days (n = 5).

on Alg was achieved by 1-(3-dimethylaminopropyl)-3-ethyl-carbodiimide hydrochloride (EDC)/N-hydroxysuccinimide (NHS), The successful synthesis of Alg-BP was confirmed by the proton nuclear magnetic resonance (^{1}H NMR) spectrum (Fig. S1). The distinct peaks at around 2.4 ppm and 1.8 ppm corresponds to the protons of the methylene groups in BPs, and the degree of BP substitution was then calculated to be approximately 7 %. For SF, which provides ~18 mol% carboxyl functionality of the available amino acids in the protein [32], GSH was grafted via a similar approach, and the successful conjugation was verified through a reduced glutathione colorimetric assay kit (Fig. S2). Hydrogels were cast by rapidly mixing the stock solutions of Alg-BP, SF-GSH, SF-MA, and Ca^{2+}/Mg^{2+}. The electrostatic interaction and dynamic coordination between Alg-BP and cations led to the swift formation of the primary hydrogel network, while the thiol-ene click reaction between GSH and MA groups on SF created the interpenetrating polymer network (IPN). We investigated the viscoelasticity of the Alg hydrogels via rheological tests and found that all hydrogels had similar storage moduli (G′) of ~1000 Pa, which were higher than their corresponding loss moduli (G″) (~100 Pa) (Fig. S3). Interestingly, despite the potential for extra crosslinking and a denser network with the presence of Mg^{2+} or SF, they might also interfere with the interaction between Alg-BP and Ca^{2+} through competition or hindrance. Therefore, all the hydrogels with the same Ca^{2+} concentration (7.5 mM) displayed similar moduli despite the addition of Mg^{2+} or SF. Frequency sweep analysis (10^{-1} Hz–10 Hz) further illustrated that the G′ and G″ of these hydrogels exhibited frequency dependence, underscoring the dynamic nature of the networks. This phenomenon was even more pronounced in the SF-containing hydrogels (Alg/SF and Alg-Mg/SF), which can be attributed to the abundant non-covalent interactions in the SF networks (Fig. 2a and b).

Swelling behavior holds significant relevance in biomedical applications of hydrogels, particularly for nerve implants, as excessive

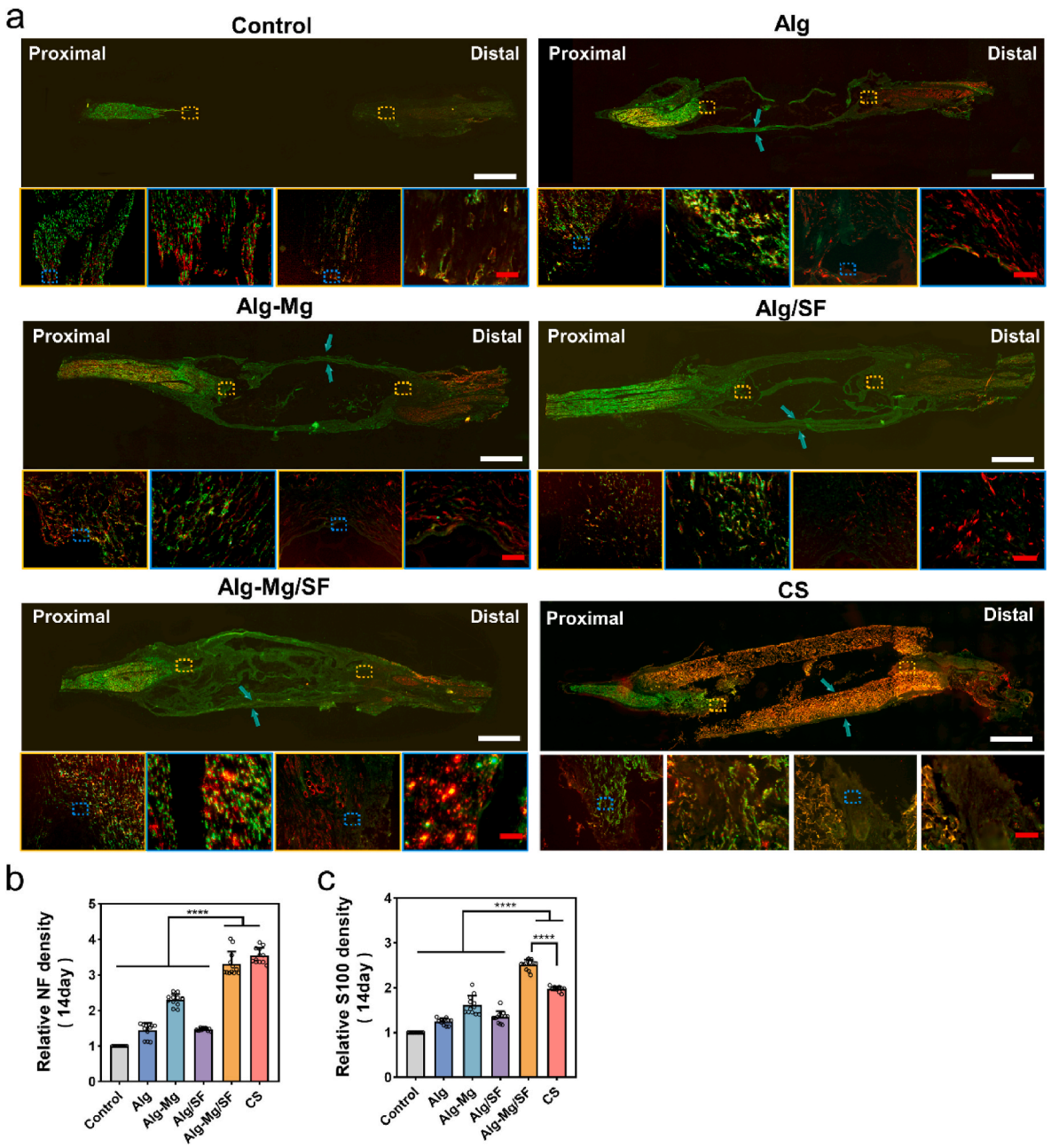

Fig. 3. Alg-Mg/SF hydrogel stimulated extensive neurite ingrowth and SCs infiltration. (a) Full-length longitudinal sections of nerve samples 2 weeks post-operation were immunostained with anti-NF (green) or anti-S100 (red) antibodies, blue arrow: hydrogel conduit; scale bars, 2000 μm in the upper row and 100 μm in the lower row, respectively. **(b–c)** Quantification of the relative intensity of NF (b) and S100 (c) in the longitudinal sections; (n = 15); $^{****}p < 0.0001$.

swelling may cause compression of surrounding nerve tissues [33]. As depicted in Fig. 2c, the swelling ratio of Alg, Alg-Mg, Alg/SF and Alg-Mg/SF hydrogels decreased in the order of 200 %–120 %. Subsequently, we studied the cross-sectional interior structures of the hydrogels using scanning electron microscopy (SEM) and observed that the pore diameters of Alg/SF and Alg-Mg/SF IPN hydrogels were significantly smaller than those of Alg and Alg-Mg hydrogels (Fig. 2d and e). We also evaluated the hydrophilicity of the hydrogels using contact angle tests. Although all hydrogel samples demonstrated small contact angles of ~10°, the contact angles of Alg-Mg and Alg-Mg/SF hydrogels were slightly higher than those of Alg and Alg/SF hydrogels (Fig. 2d,f). Moreover, we evaluated the long-term release capacity of Mg^{2+} for Alg-Mg hydrogels and Alg-Mg/SF IPN hydrogels. The results showed that both groups sustained continuous release of Mg^{2+} during the two-week release study, and the presence of SF further slowed down the release of Mg^{2+} (Fig. 2g). To verify the mechanical properties of the hydrogel conduit for transplantation, we assessed both suture strength and tensile strength of the hydrogels (Fig. S4). The results indicate that both the suture strength and tensile strength for each hydrogel group were approximately 0.4 N and 1 N, respectively. These values have also been reported in previous studies as sciatic nerve implants [34], suggesting that our hydrogel conduit possesses sufficient mechanical strength for transplantation.

3.2. *Cell-adaptable Alg-Mg/SF hydrogel promotes axonal regeneration and remyelination after PNI*

To evaluate the cytocompatibility of the hydrogels, we initially cultured primary rat dorsal root ganglia (DRG) neurons with a variety of Mg^{2+} contentions and observed that Mg^{2+} induced neurite outgrowth in

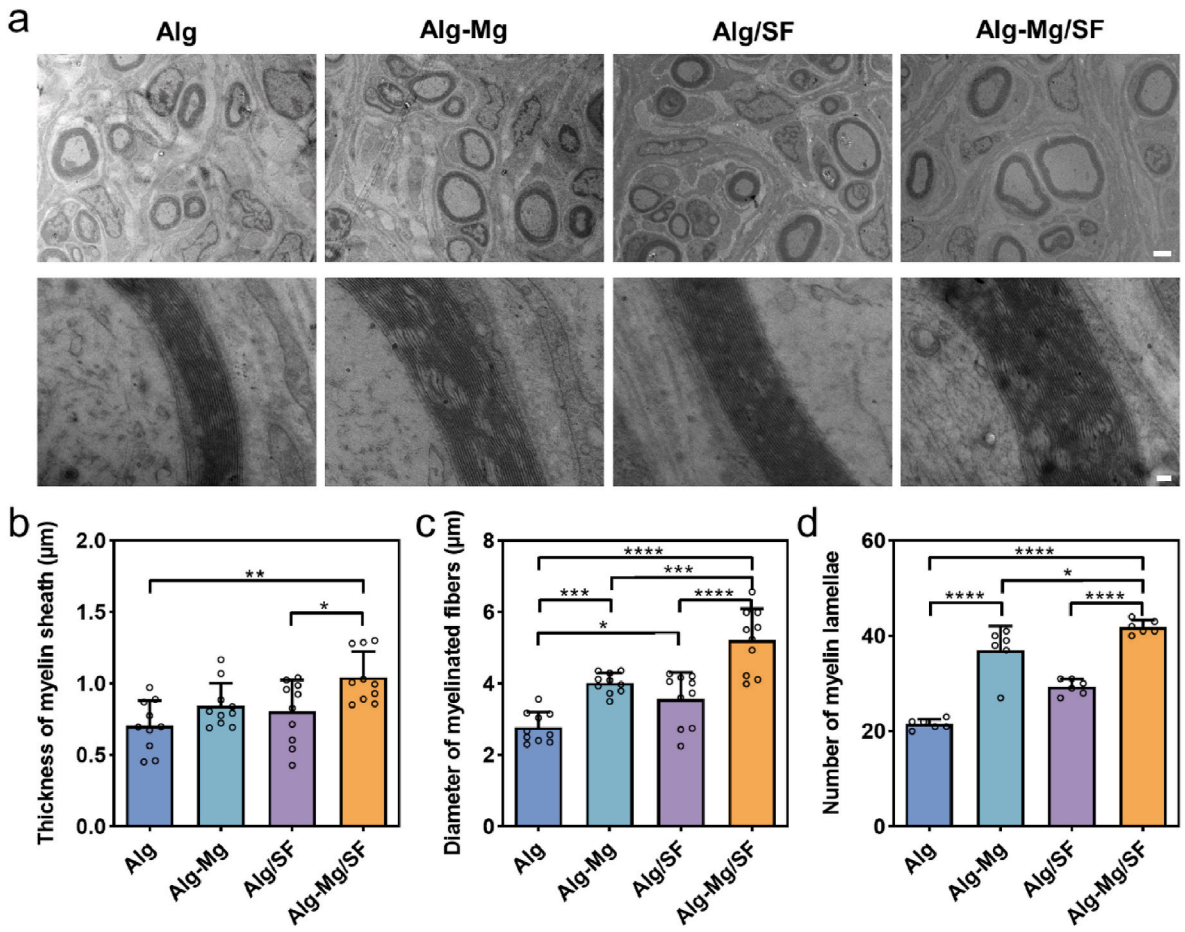

Fig. 4. Alg-Mg/SF hydrogel promoted peripheral myelination in PNI rats. (a) TEM images of transverse sections of regenerated nerve fibers 8 weeks post-surgery; scale bars, 2 μm in the upper row and 100 nm in the lower row, respectively. **(b–d)** Histograms showing the average thickness of regenerating myelin sheath (b), the diameter of myelinated axons (c), and the numbers of myelin lamellae (d) in Alg, Alg-Mg, Alg/SF, Alg-Mg/SF groups (n = 3); $^{*}p < 0.05$, $^{**}p < 0.01$, $^{***}p < 0.001$, $^{****}p < 0.0001$.

a concentration-dependent manner. Notably, cells treated with 10–40 mM Mg^{2+} displayed higher axonal growth densities and longer axonal lengths, whereas Mg^{2+} concentrations exceeding 40 mM significantly inhibited axonal outgrowth (Fig. S5). Therefore, the amount of Mg^{2+} released from the hydrogels should be within the safe and effective range. Next, we encapsulated SCs in the hydrogels and cultured them for 1, 4, or 7 days. The majority of cells in all groups remained viable, and the Alg-Mg/SF group exhibited better cell viability compared to the Alg group (Fig. S6). Similarly, by co-culturing macrophages with hydrogels, the survival rate of each group was as high as 99 % (Fig. S6), further confirming the good biocompatibility of the hydrogels. Moreover, using CCK8 experiments, we also found that the proliferation of both SCs and macrophages was promoted by the hydrogels (Fig. S6). Finally, as shown in Fig. S7, 0.5 h after cell seeding, a larger number of RAW264.7 cells adhered onto the Alg/SF and Alg-Mg/SF hydrogels compared to the other groups, indicating that the addition of SF components may facilitate early cell adhesion. However, no significant difference was observed on SCs upon different groups. We subsequently conducted co-culture of SCs and macrophages with the hydrogels, respectively, demonstrating that the Alg-Mg/SF hydrogel effectively promoted the secretion of neurotrophic factors by SCs and the pro-regeneration polarization of macrophages (Fig. S7). These factors may collectively contribute to the enhanced nerve regeneration.

To further explore the interaction between cells and hydrogels, we encapsulated DRG neurons in the hydrogels for 3D culture, and the neurons well extended in each group of hydrogels after 3D culture for 3 days. Notably, neurons displayed the lengthiest axons in the Alg-Mg/SF hydrogels, highlighting remarkable cell adaptability of our Alg-BP hydrogel (Figs. S8a and b). Subsequently, we introduced SCs onto the hydrogel surface, prompting their migration into the interior driven by the gradient of nerve growth factor (NGF) concentration. Notably, in Alg-Mg/SF hydrogels, SCs exhibit enhanced migration to deeper regions (Figs. S8c and d), indicating that Alg-Mg/SF exhibited a more robust dynamic network structure compared to the other groups, which positively influenced cell growth and migration.

Individual hydrogels were then customized as cylindrical nerve conduits using molds, and these hydrogel conduits were implanted into the 10-mm nerve defect sites of SD rats (Fig. S9). All animals underwent successful surgery and survived until sacrifice without any apparent surgical complications. The regenerated nerve bridges in each group were harvested at 1, 2, and 8 weeks after surgery, respectively, and immunohistostaining was carried out to evaluate the regeneration outcomes (Fig. 3a and S10). Remarkably, after only 2 weeks, a substantial number of regenerating neurites had already approached the distal stump in the Alg-Mg/SF group, whereas little regeneration was observed in other groups at the same time point (Fig. S11). After 8 weeks, the NF-positive nerve fibers were regenerated from the proximal stump in all the groups except the blank control. The Alg-Mg/SF group almost completely bridged the defect with regenerated nerve fibers, and extensive neurofilament ingrowth into the Alg/SF and Alg-Mg hydrogels was observed. In contrast, the neurites in the Alg group remained far from the distal stump with cyst formation, revealing the remarkable contributions of Mg^{2+} and SF in effective neural regeneration. Furthermore, quantitative analyses showed higher relative NF and S100

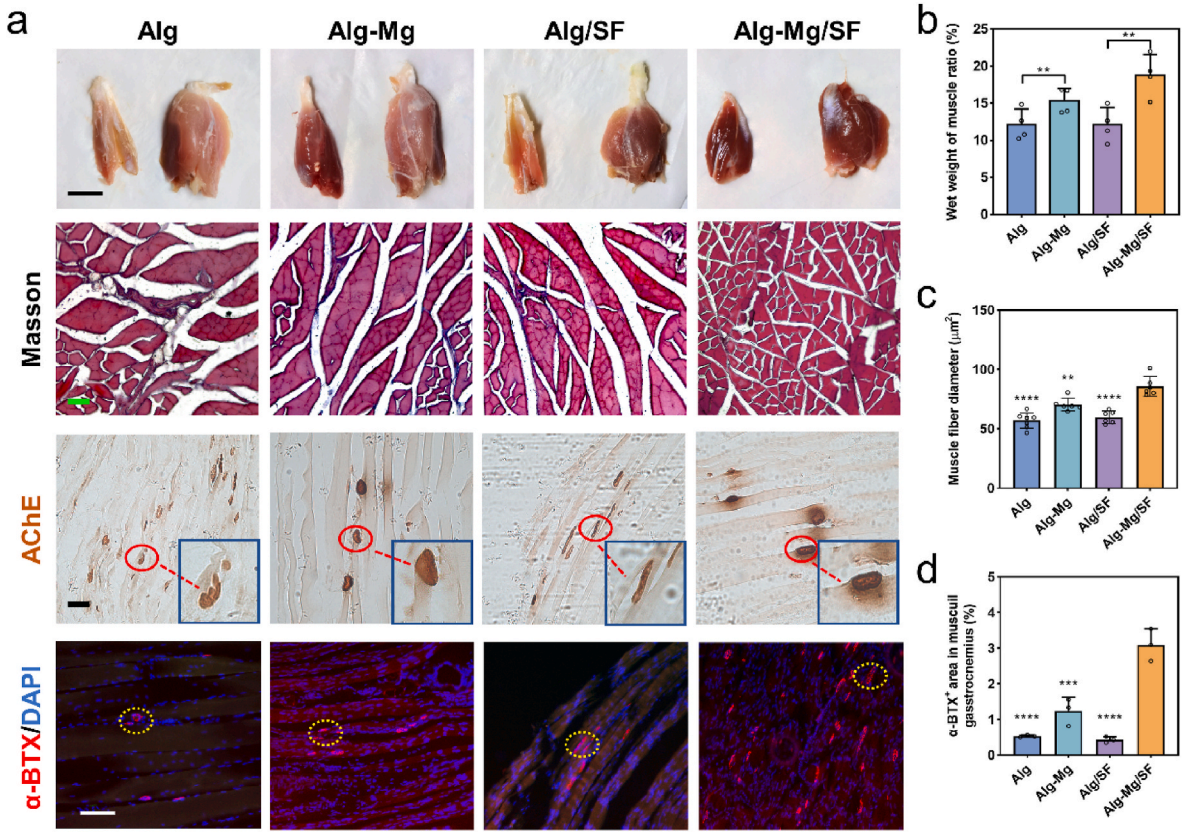

Fig. 5. Alg-Mg/SF hydrogel facilitated muscle recovery from atrophy at 8 weeks post hydrogel implantation. (a) Representative images of gastrocnemius muscles of experimental side (left) and normal side (right); scale bar = 1000 μm, and the transverse sections of the muscles stained with Masson's trichome and acetylcholinesterase (AChE) staining, respectively; scale bar = 50 μm. The immunostaining of α-BTX showed the regeneration of neuromuscular junctions; scale bar = 100 μm. **(b)** Wet weight muscle ratio of the Alg, Alg-Mg, Alg/SF, Alg-Mg/SF groups (n = 3); $^{**}p < 0.01$. **(c–d)** The diameter of muscle fibers (c) and α-BTX$^+$ area (d) in muscull gastrocnemius sections of the Alg, Alg-Mg, Alg/SF, Alg-Mg/SF groups (n = 3); $^{**}p < 0.01$, $^{***}p < 0.001$, $^{****}p < 0.0001$ compared to the Alg-Mg/SF group.

intensities in the Alg-Mg/SF group, suggesting that the hydrogels effectively enhanced neurite outgrowth and SCs infiltration (Fig. 3b and c). This finding was further confirmed by the transverse section of the regenerating nerves, where significantly more nerve fibers and S100$^+$ SCs were observed in the Alg-Mg/SF group (Fig. S12), followed by Alg-Mg, Alg/SF, Alg, and the control groups. Additionally, the increased co-localization of NF and S100 staining in the Alg-Mg/SF revealed better remyelination of the regenerated nerve fibers. It is noteworthy that at 7 and 14 days, while the Alg-Mg/SF hydrogel group had fewer nerve fibers compared to the chitosan catheter group, it exhibited a higher count of S100$^+$ cells.

The myelination of regenerating axons is of great importance in neural signaling and is associated with restoring functions after PNI [35]. We collected nerve samples 8 weeks post-operation and used transmission electron microscopy (TEM) to visualize the ultra-thin cross-sections of regenerated nerves (Fig. 4a). Three parameters, namely myelin thickness, diameter of myelinated fibers, and number of myelin lamellae, were evaluated (Fig. 4b–d). Abundant clusters of regenerated myelinated fibers were observed, surrounded by clear, thick, and electron-dense myelin sheaths in the Alg-Mg/SF group. The Alg-Mg group also exhibited good remyelination in terms of the number and diameter of the myelinated axons and the thickness of the new myelin sheath. Although the Alg/SF group displayed better remyelination than the Alg group, it was not as efficient as that in the Alg-Mg/SF group. The blank control group was not included in this characterization due to rare axon regeneration. Despite spontaneous remyelination likely occurring after PNI, the low efficiency remains a matter of concern. In this study, the Alg-Mg/SF hydrogels provided a permissive environment in the lesion site, favoring axonal regeneration and myelin regeneration. Moreover, our previous research found that fibroblasts can promote repair after peripheral nerve damage through paracrine effects, which promotes myelination in sciatic nerves [36]. Here, we further investigated the regulatory effect of each group of hydrogels on the paracrine effect of fibroblasts. Through the co-culture of fibroblasts and hydrogels, we found that the expression of RTN3 and RAB21, genes regulating exosome release, was upregulated by the Alg-Mg/SF hydrogel group (Fig. S13), which indicated that Alg-Mg/SF hydrogel could promote the release of fibroblastic exosomes and may also contribute to the remyelination after peripheral nerve injury.

3.3. Cell-adaptable Alg-Mg/SF hydrogel facilitates muscle recovery from atrophy

The gastrocnemius muscle, innervated by the sciatic nerve, serves as an indicator of the degree of nerve regeneration after injury [37]. Despite all the groups experiencing muscle atrophy 8 weeks post-operation, reinnervation facilitated by hydrogel implantation significantly improved the condition. As depicted in Fig. 5a, the Alg and Alg/SF groups displayed considerable muscle shrinkage compared to the Mg-containing groups (Alg-Mg and Alg-Mg/SF), which demonstrated better recovery from atrophy. We further quantified the ratio of muscle wet weight (injured side/healthy side) and found that the muscles in the Alg-Mg/SF group had the least atrophy (19.0 % ± 0.8 %) among all groups (Fig. 5b), consistent with the trend of nerve regeneration. We subsequently studied the morphology of the gastrocnemius muscles using Masson's trichrome staining and observed that the Alg-Mg/SF group displayed the largest diameter of muscle fibers and the smallest cross-sectional area of collagen fibers (Fig. 5c and S14). In addition, the

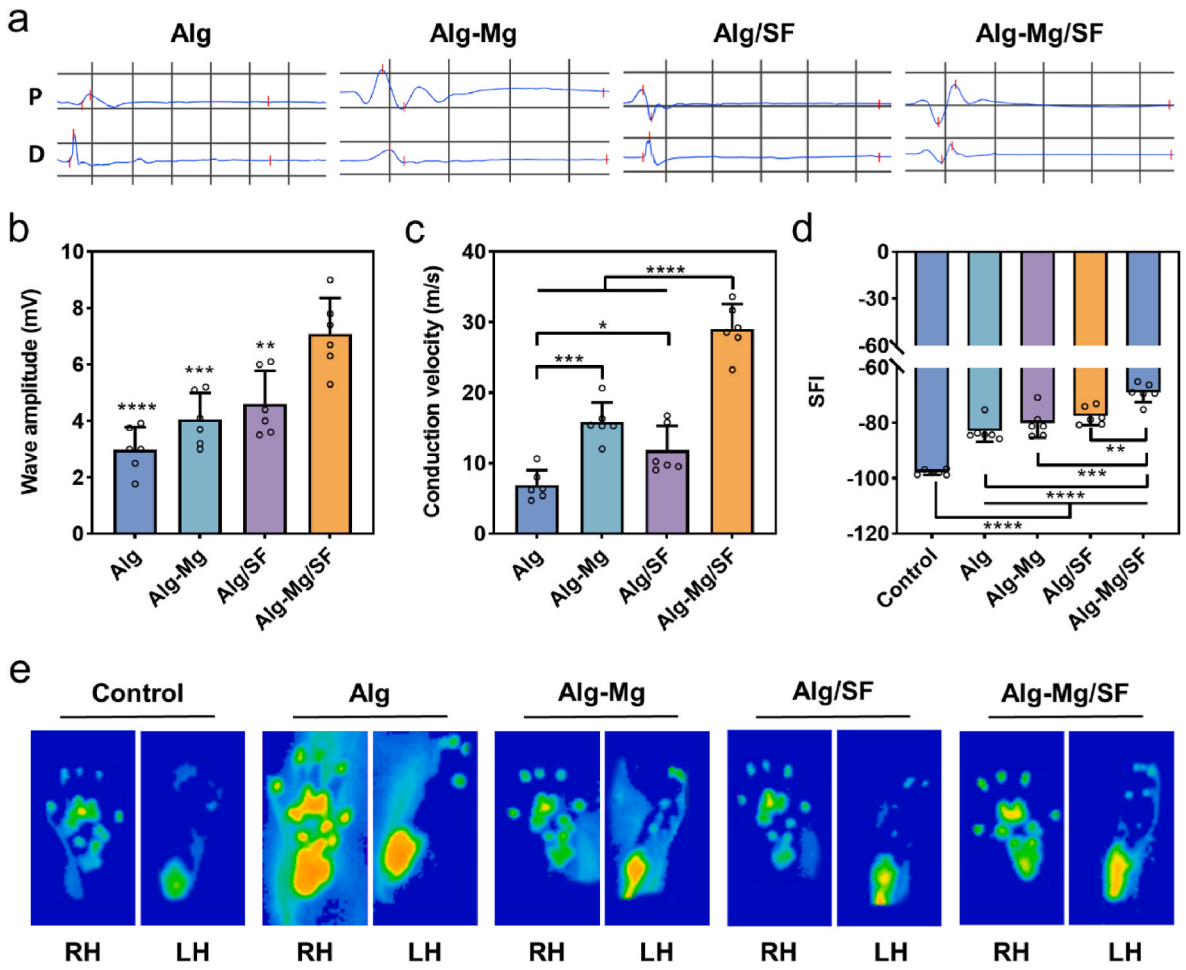

Fig. 6. Alg-Mg/SF hydrogel promoted functional recovery 8 weeks post-operation. (a) Electrophysiological assessment of CMAP in sciatic nerves treated with different hydrogels, "P" represents proximal, and "D" represents distal. **(b)** CMAP detected in the injured side of animals (n = 6); $^{**}p < 0.01$, $^{***}p < 0.001$ $^{****}p < 0.0001$ compared to the Alg-Mg/SF group. **(c)** Motor nerve conduction velocities were detected in the injured side of animals (n = 6); $^{*}p < 0.05$, $^{***}p < 0.001$, $^{****}p < 0.0001$. **(d)** SFI calculated from the walking track (n = 6); $^{**}p < 0.01$, $^{***}p < 0.001$, $^{****}p < 0.0001$. **(e)** Representative images of footprints automatically captured by the catwalk gait analysis system.

Alg/SF group demonstrated a larger diameter of muscle fibers and a smaller cross-section area of collagen fibers compared to the Alg group. Acetylcholinesterase (AChE) staining was performed to detect the endplate of gastrocnemius muscles [38]. Once again, the Alg-Mg/SF group demonstrated optimal nerve regeneration and muscle function, as evidenced by the increased number, area, and color of motor endplates. The sections of gastrocnemius muscles were also stained with α-bungarotoxin (α-BTX), an acetylcholine receptor-binding neurotoxin, to detect the regeneration of neuromuscular junctions (NMJs) [39], and a substantially greater α-BTX/DAPI ratio was found in the Alg-Mg/SF group (Fig. 5d and S15).

3.4. Cell-adaptable Alg-Mg/SF hydrogel promotes nerve functional recovery after PNI

To verify complete and successful peripheral regeneration, we next determined rat motor activity through electromyography (EMG) at 8 weeks post-surgery. No detectable compound muscle action potential (CMAP) amplitude was recorded in animals that received no hydrogel implantation due to the lack of nerve regeneration, while all other groups demonstrated partially functional recovery. The Alg-Mg/SF group exhibited the highest onset-to-peak amplitudes of CMAP (7.08 ± 1.17 mV), followed by the Alg/SF (4.60 ± 1.07 mV), Alg-Mg (4.05 ± 0.85 mV), and Alg (2.99 ± 0.73 mV) groups (Fig. 6a and b). Moreover, substantially higher nerve conduction velocity (NCV) was found in the Alg-Mg/SF group (29.03 ± 3.24 m/s) (Fig. 6c). The Alg-Mg group (15.84 ± 2.53 m/s) exhibited better NCV than the Alg-SF group (11.87 ± 3.15 m/s), whereas the Alg group (6.91 ± 1.96 m/s) displayed significantly lower NCV than the other groups. We also captured the footprints and gaits of the animals in all groups at 8 weeks using a catwalk gait analysis system and determined the sciatic nerve function through walking track analysis and assessed in the sciatic function index (SFI) of the animals in all groups at 8 weeks. The SFI value in the Alg-Mg/SF group was −69.03 ± 3.20, significantly higher than those of the other groups (Fig. 6d). In contrast, the SFI value in the Alg group was only −97.78 ± 0.85, indicating an almost complete loss of neural function. Moreover, the walking track analysis results showed that both the intensity and contact area of the left hind (LH) paws were significantly reduced after injury compared to those of the uninjured right hind (RH) paws in all groups, while the application of Alg-Mg/SF hydrogels effectively attenuated these reductions (Fig. 6e). An electric potential is activated with electrical or neurological stimulation of nerve cells, and hence no detectable amplitude was obtained in the EMG of blank control group.

3.5. Cell-adaptable Alg-Mg/SF hydrogel promotes nerve regeneration through the reconstruction of microenvironment

To understand the mechanism underlying the enhanced nerve regeneration induced by the Alg-Mg/SF hydrogel, we employed RNA

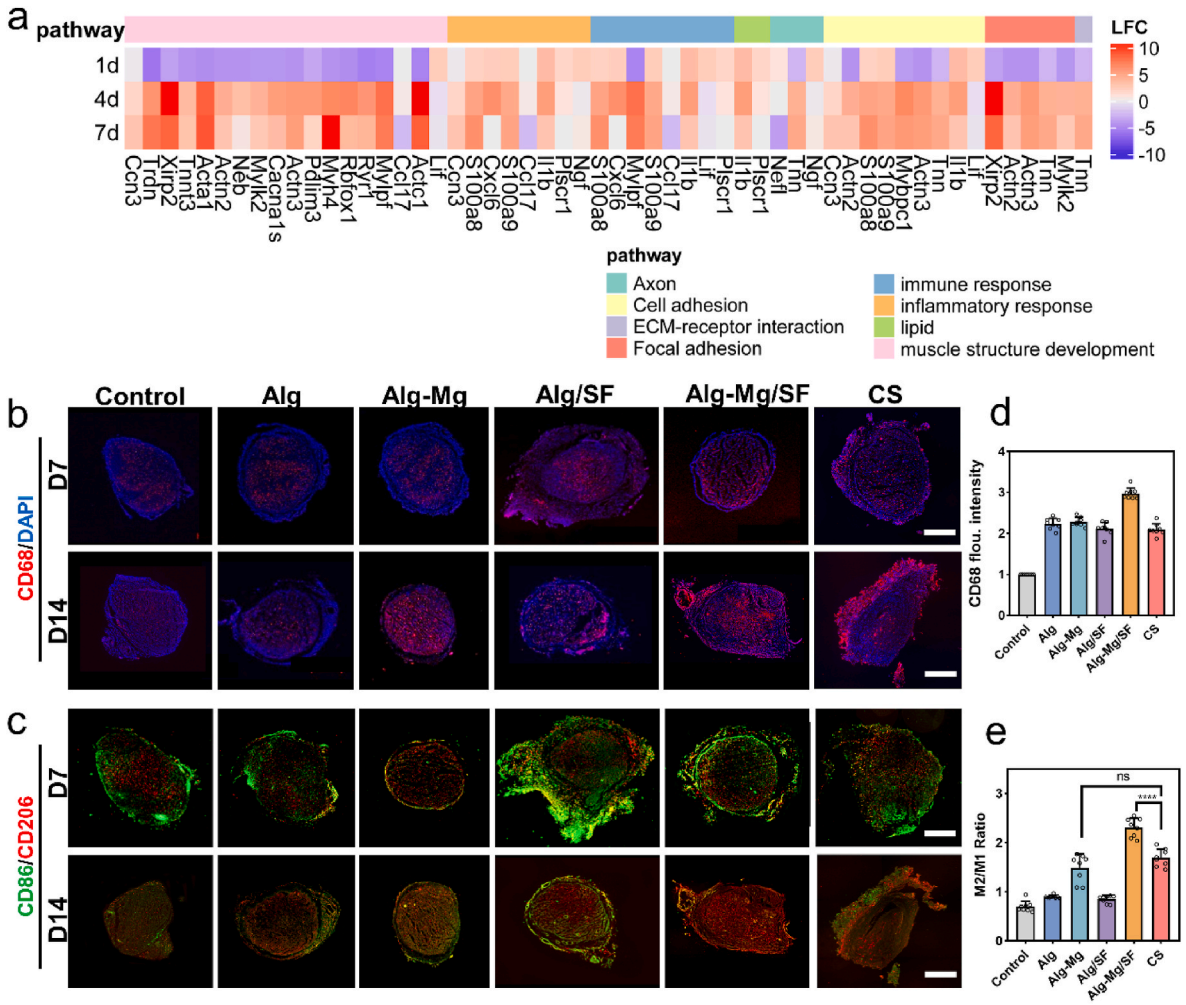

Fig. 7. Alg-Mg/SF hydrogel promoted nerve regeneration through the reconstruction of microenvironment. (a) Heatmap of gene expression determined by mRNA sequencing comparing nerve bridges in the Alg-Mg/SF collected at different time points. **(b–c)** Macrophage infiltration and polarization within the hydrogels at 7 and 14 days were characterized by immunofluorescent staining for CD68 (pan-macrophage), CD86 (M1, pro-inflammatory) and CD206 (M2, anti-inflammatory); scale bar = 500 μm. **(d)** The fluorescence intensity of CD68 staining indicated the number of infiltrating macrophages in the hydrogels on day 14 (as determined from the cross-sectional sections) (n = 8). **(e)** The ratio of M2/M1 macrophages in the hydrogels on day 14 (n = 8); $^{****}p < 0.0001$.

sequencing to determine the transcriptional changes of the nerve regeneration bridges at 1, 4, and 7 days after surgery. Heat maps of mRNA expression profiles derived from hierarchical clustering analysis of transcriptome data indicated that compared with the destroyed tissues at day 1, the Alg-Mg/SF hydrogel significantly upregulated gene expression related to focal adhesion, axon regeneration, and muscle structure development at day 7 (Fig. 7a). In particular, genes associated with immune response and inflammatory response were upregulated in the first several days and downregulated afterward, revealing the potential role of the Alg-Mg/SF hydrogels in the modulation of local inflammatory response, an important pathophysiological response to PNI that may determine the injury's outcome. Consequently, we subsequently investigated the infiltration and polarization of macrophages at the nerve regeneration bridges by immunofluorescent staining for CD68, CD86, and CD206, respectively. Numerous $CD68^+$ cells accumulated in the nerve bridge of hydrogel-implantation groups at 7 and 14 days, whereas significantly fewer cells were observed in the PNI group with no therapeutic interventions (Fig. 7b and c), implying that the hydrogels were effective in promoting cell migration for recruitment. The results further showed that the hydrogels, especially the Alg-Mg/SF hydrogels, rapidly recruited macrophages in the short term and then promoted their M2 transition, as evidenced by the dominant presence of $CD86^+$ cells at day 7 and more $CD206^+$ staining at day 14. These findings surpass those observed in the commercial chitosan conduit group (Fig. 7d). Statistical analysis further showed that the ratio of M1/M2 in the Alg-Mg/SF group was significantly lower than that of other groups at both 7 and 14 days (Fig. 7e and S16).

To systematically explore the role of the hydrogel components in nerve regeneration over time, we employed a linear model to extract differentially expressed (DE) genes (Table S3) affected by each parameter independently, disregarding the influence of other background parameters (Fig. 8a). This approach allowed us to reveal DE genes affected by Mg^{2+} independently of the addition of SF or different time points. The resulting Venn diagram strikingly displayed a significant discrepancy in the number of DE genes for the different parameter comparisons (Fig. 8b). Unsurprisingly, the time of regeneration was the major driver of DE genes, followed by the incorporation of Mg^{2+} and SF. We further conducted all pairwise comparisons, revealing varying numbers of DE genes ranging from 0 to over 700. However, the latter number was considerably lower than that of the decoupled gene sets (Fig. 8c), suggesting the superposition of different material sensing mechanisms. Subsequently, we mapped the DE gene sets to different pathways and discovered that, besides the immune and inflammatory pathways discussed earlier, the adaptable hydrogels may also regulate the lipid metabolism of the cells (Fig. 8d). The immune response and inflammatory response at the early stages after damage is essential for

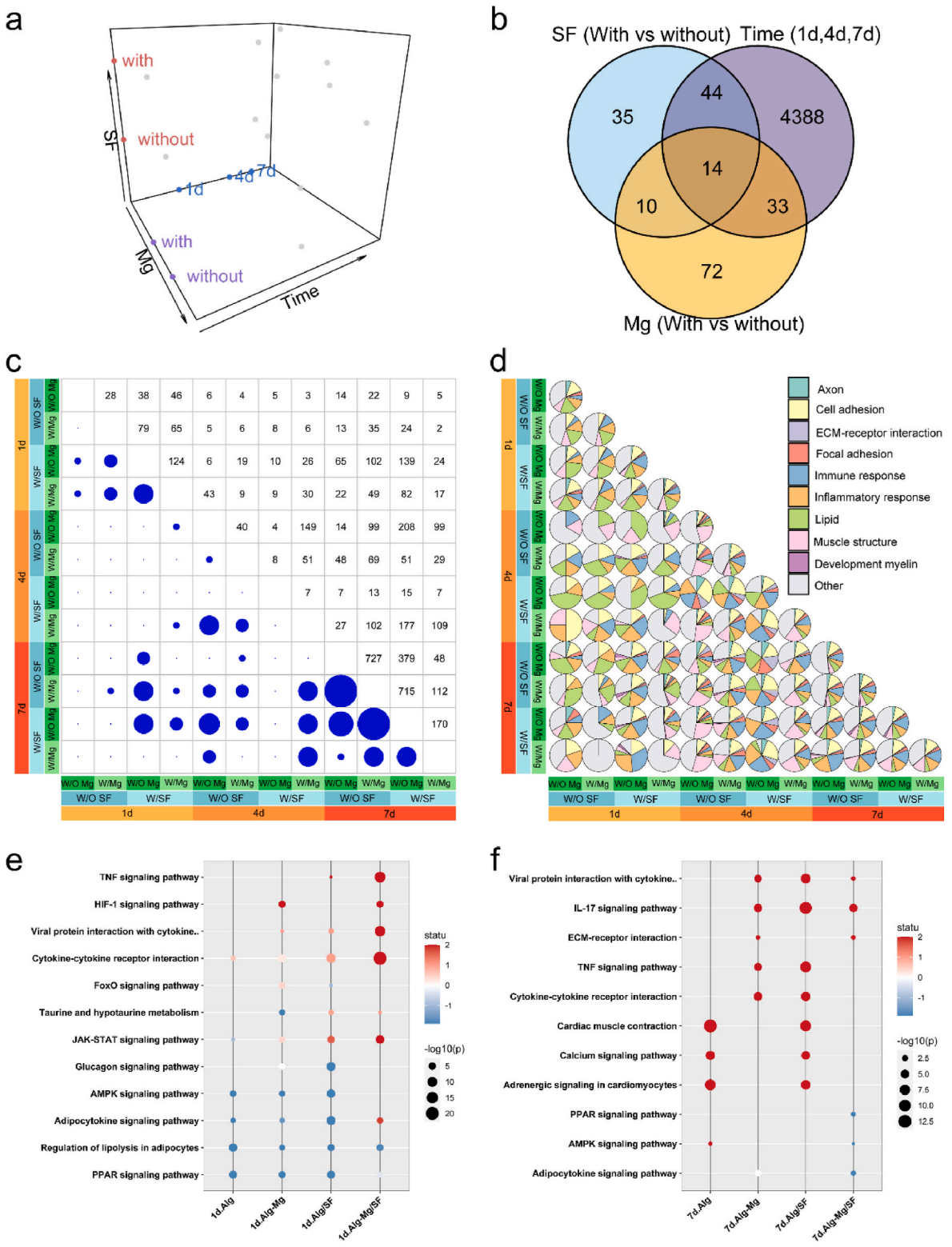

Fig. 8. Cell-adaptable Alg-Mg/SF hydrogel regulated the transcriptome of surrounding tissues after PNI. (a) Schematic of experimental conditions of PNI treatment using hydrogels. **(b)** Venn diagrams of DE genes for each material parameter comparison after controlling for other parameters. The numbers of DE genes shared by two parameters are indicated in the overlap in circles. **(c)** Number of DE genes in nerve tissues for all pairwise material comparisons. The circle area corresponds to the number of DE genes as indicated in the symmetrical position in the chart. **(d)** Pie chart of the DE genes in nerve tissues related to different pathways. **(e–f)** The gene enrichment KEGG pathway analysis of nerve regeneration bridges at 1- and 7-days post-operation, respectively.

efficient immunity, which reconstruct microenvironment benefits tissue healing. *De novo* lipid synthesis and metabolism could be used to construct the myelin sheath, which plays an essential role in peripheral regeneration. To further understand the signal pathway associated with DE genes, Kyoto Encyclopedia of Genes and Genomes (KEGG) pathway enrichment analysis identified that TNF signaling, calcium signaling,

MAPK signaling pathways, and cytokine-cytokine receptor interactions was the most significantly enriched functional pathway (Fig. 8e and f). These findings provide valuable insights into the intricate mechanisms underlying nerve regeneration facilitated by the cell-adaptable Alg-Mg/SF hydrogel in a time-dependent manner.

4. Discussion

It is known that SF can form self-assembled hydrogels due to the formation of β-sheet crystals [17]. However, this network is generally too tough to match the soft mechanical properties of the native neural ECM [40]. Therefore, we crosslinked SF via a biorthogonal thiol-ene click reaction, and the presence of hydrophilic Alg network may hinder the formation of antiparallel β-sheet crystallites in SF. Moreover, compared with the well-investigated electrostatic interactions between Alg and Ca^{2+}, Mg^{2+} exhibits a weaker binding affinity. The conjugation of BPs to Alg introduced extra dynamic coordination between the polymer backbone and metallic cations, and this more dynamic interaction may further contribute to the sustained release of the bioactive cations. Previous works have fabricated hyaluronic acid (HA)-based hydrogels for the delivery of Mg^{2+} to promote tissue regeneration. However, the interactions between HA backbone and Mg^{2+} were not sufficient to support a stable hydrogel network, and thus relatively large amount free BPs were added to form nanoparticles to reinforce the crosslinking [24]. Our work used the BP-modified alginate which can form stronger interaction with cations, thereby eliminating the potential risks of heterotopic calcium deposition caused by free BP. This makes our hydrogels safer and more suitable for application at the sites of neural injury.

Adaptable hydrogels are polymer networks crosslinked by dynamic bonds that can be broken and re-formed in a reversible manner without external triggers. In the context of cell culture, the polymer blocks can be rearranged to generate enough space for cell deformation. This feature creates a more permissive environment for cells to interact with the hydrogel matrix, facilitating crucial cellular processes for tissue regeneration, such as migration, spreading, mechanosensing, and differentiation. After PNI, SCs need to migrate from both proximal and distal nerve stumps into the nerve bridge and guide axon regeneration after PNI [41]. As expected, our Alg-Mg/SF hydrogels effectively facilitated SCs infiltration and neurite outgrowth within 8 weeks. Moreover, our results emphasized the importance of the biochemical microenvironment in nerve regeneration. Although the Alg hydrogels exhibited similar structural and mechanical properties to the Alg-Mg ones, the lack of bioactivity (Mg^{2+} supplementation) led to poor neurite ingrowth, with regenerated neural tissues only observed on the surface of the Alg hydrogels. Similarly, as SF can support cell adhesion, the Alg-Mg/SF hydrogels demonstrated better neurite ingrowth than the Alg-Mg hydrogels, particularly at the early time points.

After a sciatic nerve injury, the observed atrophy and functional decline in the gastrocnemius muscle can be attributed to the compromised neural transmission integrity. The sciatic nerve, responsible for controlling the posterior muscles of the thigh and calf, as well as carrying sensory signals, experiences impaired neural signaling due to the injury. As a result, the gastrocnemius muscle undergoes denervation, leading to atrophy and diminished functionality. Our Alg-Mg/SF hydrogel exhibits superior efficacy in promoting axon ingrowth and SCs migration, thus accelerating nerve repair after injury. This suggests that following an injury, the sciatic nerve can more rapidly reinnervate the gastrocnemius muscle, thereby expediting the recovery of gastrocnemius muscle function. As expected, our results suggest that the efficient nerve regeneration facilitated by the Alg-Mg/SF hydrogels effectively reversed the atrophy of gastrocnemius muscles. Furthermore, previous studies used polycaprolactone-based nerve conduits and HA hydrogels for the regeneration of 10-mm sciatic nerve defect, and the CAMP values at 12 weeks after operation were 1 and 2, respectively [42], which are even lower than the values determined in the Alg-Mg/SF group at week 8. Together, these functional studies strongly suggest that the Alg-Mg/SF hydrogel effectively contributed to peripheral nerve regeneration.

Moreover, the inflammatory response is of great significance in nerve regeneration. Upon nerve injury, macrophages were initially polarized into M1 phenotype, and these cells are involved in removing degenerating axons and myelin debris, which was beneficial to nerve regeneration. Subsequently, owning to immunomodulatory effect of the released Mg^{2+}, an increasing number of macrophages are promoted towards M2 transition, contributing to SCs recruitment, myelinization and axonal extension [43]. Therefore, the Alg-Mg/SF hydrogel can achieve sequential regulation of macrophage recruitment and polarization to effectively accommodate the demands of regeneration over time.

5. Conclusion

In summary, we have developed an Mg-containing adaptable IPN hydrogel with Alg-BP and SF for peripheral nerve regeneration, shedding light on the underlying mechanisms. These hydrogels possess unique bioactivity and impressive dynamic properties that effectively promote SCs infiltration and neurite ingrowth in vivo, leading to efficient muscle recovery from atrophy and nerve functional recovery. Moreover, the cell-adaptable Alg-Mg/SF hydrogel can rapidly recruit macrophages and subsequently promote their M2 transition. Given the crucial roles of both SCs and macrophages in the regenerative microenvironment, this study highlights the potential of adaptable hydrogels as a promising approach for the reconstruction of microenvironment and the clinical treatment of PNI.

Conflict of interests

The authors declare no conflict of interests.

Ethics approval and consent to participate

The study received approval from the institutional review board of Nantong University.

CRediT authorship contribution statement

Yisheng Gao: Investigation, Data curation, Formal analysis. **Yingyu Wang:** Investigation, Validation. **Jianye Zhang:** Investigation, Software. **Miao Zhang:** Investigation. **Chaolun Dai:** Investigation. **Yang Zhang:** Investigation. **Luzhong Zhang:** Software. **Liming Bian:** Supervision, Writing – review & editing. **Yumin Yang:** Funding acquisition, Supervision, Writing – review & editing, Conceptualization. **Kunyu Zhang:** Conceptualization, Funding acquisition, Methodology, Writing – original draft, Writing – review & editing. **Yahong Zhao:** Funding acquisition, Project administration, Supervision, Writing – original draft, Writing – review & editing.

Declaration of competing interest

The authors declare no conflict of interests.

Acknowledgements

This work was supported by National Natural Science Foundation of China (32230057; 32271385; 32371400), Natural Science Foundation of Jiangsu Province (BK20231338) and the Priority Academic Program Development of Jiangsu Higher Education Institutions (PAPD) (21KJA 430011).

Appendix A. Supplementary data

Supplementary data to this article can be found online at https://doi.org/10.1016/j.bioactmat.2023.10.026.

References

[1] J. Noble, C.A. Munro, V.S. Prasad, R. Midha, Analysis of upper and lower extremity peripheral nerve injuries in a population of patients with multiple injuries, J. Trauma 45 (1998) 116–122, https://doi.org/10.1097/00005373-199807000-00025.

[2] T. Kornfeld, P.M. Vogt, C. Radtke, Nerve grafting for peripheral nerve injuries with extended defect sizes, Wien Med. Wochenschr. 169 (2019) 240–251, https://doi.org/10.1007/s10354-018-0675-6.

[3] D.H. Smith, J.C. Burrell, K.D. Browne, K.S. Katiyar, M.I. Ezra, J.L. Dutton, J. P. Morand, L.A. Struzyna, F.A. Laimo, H.I. Chen, J.A. Wolf, H.M. Kaplan, J. M. Rosen, H.C. Ledebur, E.L. Zager, Z.S. Ali, D.K. Cullen, Tissue-engineered grafts exploit axon-facilitated axon regeneration and pathway protection to enable recovery after 5-cm nerve defects in pigs, Sci. Adv. 8 (2022), eabm3291, https://doi.org/10.1126/sciadv.abm3291.

[4] I. Gilron, R. Baron, T. Jensen, Neuropathic pain: principles of diagnosis and treatment, Mayo Clin. Proc. 90 (2015) 532–545, https://doi.org/10.1016/j.mayocp.2015.01.018.

[5] G. Raisman, Sniffing out new approaches to spinal cord repair, Nat. Med. 6 (2000) 382–383, https://doi.org/10.1038/74638.

[6] N.P. Patel, K.A. Lyon, J.H. Huang, An update-tissue engineered nerve grafts for the repair of peripheral nerve injuries, Neural Regen Res 13 (2018) 764–774, https://doi.org/10.4103/1673-5374.232458.

[7] L. Kong, X. Gao, Y. Qian, W. Sun, Z. You, C. Fan, Biomechanical microenvironment in peripheral nerve regeneration: from pathophysiological understanding to tissue engineering development, Theranostics 12 (2022) 4993–5014, https://doi.org/10.7150/thno.74571.

[8] M.K. Jha, J.V. Passero, A. Rawat, X.H. Ament, F. Yang, S. Vidensky, S.L. Collins, M. R. Horton, A. Hoke, G.A. Rutter, A. Latremoliere, J.D. Rothstein, B.M. Morrison, Macrophage monocarboxylate transporter 1 promotes peripheral nerve regeneration after injury in mice, J. Clin. Invest. 131 (2021), e141964, https://doi.org/10.1172/JCI141964.

[9] Y. Matsui, K. Kadoya, Y. Nagano, T. Endo, M. Hara, G. Matsumae, T. Suzuki, Y. Yamamoto, M.A. Terkawi, N. Iwasaki, IL4 stimulated macrophages promote axon regeneration after peripheral nerve injury by secreting uPA to stimulate uPAR upregulated in injured axons, Cell. Mol. Life Sci. 79 (2022) 289, https://doi.org/10.1007/s00018-022-04310-5.

[10] J. Li, Y. Yao, Y. Wang, J. Xu, D. Zhao, M. Liu, S. Shi, Y. Lin, Modulation of the crosstalk between schwann cells and macrophages for nerve regeneration: a therapeutic strategy based on a multifunctional tetrahedral framework nucleic acids system, Adv. Mater. 34 (2022), e2202513, https://doi.org/10.1002/adma.202202513.

[11] P.L. Graney, S. Ben-Shaul, S. Landau, A. Bajpai, B. Singh, J. Eager, A. Cohen, S. Levenberg, K.L. Spiller, Macrophages of diverse phenotypes drive vascularization of engineered tissues, Sci. Adv. 6 (2020), eaay6391, https://doi.org/10.1126/sciadv.aay6391.

[12] A.D. Gaudet, P.G. Popovich, M.S. Ramer, Wallerian degeneration: gaining perspective on inflammatory events after peripheral nerve injury, J. Neuroinflammation 8 (2011) 110, https://doi.org/10.1186/1742-2094-8-110.

[13] M. Bessa-Gonçalves, C. Ribeiro-Machado, M. Costa, C. Ribeiro, J. Barbosa, M. Barbosa, S. Santos, Magnesium incorporation in fibrinogen scaffolds promotes macrophage polarization towards M2 phenotype, Acta Biomater. 155 (2023) 667–683, https://doi.org/10.1016/j.actbio.2022.10.046.

[14] L. Sun, X. Li, M. Xu, F. Yang, W. Wang, X. Niu, In vitro immunomodulation of magnesium on monocytic cell toward anti-inflammatory macrophages, Regener. Biomater. 7 (2020) 391–401, https://doi.org/10.1093/rb/rbaa010.

[15] D.C. Turner, L.A. Flier, S. Carbonetto, Magnesium-dependent attachment and neurite outgrowth by PC12 cells on collagen and laminin substrata, Dev. Biol. 121 (1987) 510–525, https://doi.org/10.1016/0012-1606(87)90187-4.

[16] H.-C. Pan, M.-L. Sheu, H.-L. Su, Y.-J. Chen, C.-J. Chen, D.-Y. Yang, W.-T. Chiu, F.-C. Cheng, Magnesium supplement promotes sciatic nerve regeneration and down-regulates inflammatory response, Magnes. Res. 24 (2011) 54–70, https://doi.org/10.1684/mrh.2011.0280.

[17] J.K. Sahoo, O. Hasturk, T. Falcucci, D.L. Kaplan, Silk chemistry and biomedical material designs, Nat. Rev. Chem (2023) 1–17, https://doi.org/10.1038/s41570-023-00486-x.

[18] K. Franze, P.A. Janmey, J. Guck, Mechanics in neuronal development and repair, Annu. Rev. Biomed. Eng. 15 (2013) 227–251, https://doi.org/10.1146/annurev-bioeng-071811-150045.

[19] K. Franze, The mechanical control of nervous system development, Development 140 (2013) 3069–3077, https://doi.org/10.1242/dev.079145.

[20] Y. Zhao, J. Liu, Y. Gao, Z. Xu, C. Dai, G. Li, C. Sun, Y. Yang, K. Zhang, Conductive biocomposite hydrogels with multiple biophysical cues regulate schwann cell behaviors, J. Mater. Chem. B 10 (2022) 1582–1590, https://doi.org/10.1039/D1TB02361F.

[21] H. Wang, S.C. Heilshorn, Adaptable hydrogel networks with reversible linkages for tissue engineering, Adv. Mater. 27 (2015) 3717–3736, https://doi.org/10.1002/adma.201501558.

[22] Z. Tong, L. Jin, J.M. Oliveira, R.L. Reis, Q. Zhong, Z. Mao, C. Gao, Adaptable hydrogel with reversible linkages for regenerative medicine: dynamic mechanical microenvironment for cells, Bioact. Mater. 6 (2021) 1375–1387, https://doi.org/10.1016/j.bioactmat.2020.10.029.

[23] K. Zhang, Q. Feng, Z. Fang, L. Gu, L. Bian, Structurally dynamic hydrogels for biomedical applications: pursuing a fine balance between macroscopic stability and microscopic dynamics, Chem. Rev. 121 (2021) 11149–11193, https://doi.org/10.1021/acs.chemrev.1c00071.

[24] K. Zhang, Z. Jia, B. Yang, Q. Feng, X. Xu, W. Yuan, X. Li, X. Chen, L. Duan, D. Wang, L. Bian, Adaptable hydrogels mediate cofactor-assisted activation of biomarker-responsive drug delivery via positive feedback for enhanced tissue regeneration, Adv. Sci. 5 (2018), 1800875, https://doi.org/10.1002/advs.201800875.

[25] J. Liang, X. Zhang, Z. Chen, S. Li, C. Yan, Thiol–ene click reaction initiated rapid gelation of PEGDA/silk fibroin hydrogels, Polymers 11 (2019) 2102, https://doi.org/10.3390/polym11122102.

[26] Y. Zhao, Y. Liang, Z. Xu, J. Liu, X. Liu, J. Ma, C. Sun, Y. Yang, Exosomal miR-673-5p from fibroblasts promotes Schwann cell-mediated peripheral neuron myelination by targeting the TSC2/mTORC1/SREBP2 axis, J. Biol. Chem. 298 (2022), 101718, https://doi.org/10.1016/j.jbc.2022.101718.

[27] Y. Zhao, J. Liu, S. Liu, P. Yang, Y. Liang, J. Ma, S. Mao, C. Sun, Y. Yang, Fibroblast exosomal TFAP2C induced by chitosan oligosaccharides promotes peripheral axon regeneration via the miR-132-5p/CAMKK1 axis, Bioact. Mater. 26 (2023) 249–263, https://doi.org/10.1016/j.bioactmat.2023.03.002.

[28] L.T.A. Hong, Y.-M. Kim, H.H. Park, D.H. Hwang, Y. Cui, E.M. Lee, S. Yahn, J.K. Lee, S.-C. Song, B.G. Kim, An injectable hydrogel enhances tissue repair after spinal cord injury by promoting extracellular matrix remodeling, Nat. Commun. 8 (2017) 533, https://doi.org/10.1038/s41467-017-00583-8.

[29] Z. Ying, C. Pan, T. Shao, L. Liu, L. Li, D. Guo, S. Zhang, T. Yuan, R. Cao, Z. Jiang, S. Chen, F. Wang, X. Wang, Mixed lineage kinase domain-like protein MLKL breaks down myelin following nerve injury, Mol. Cell 72 (2018) 457–468, https://doi.org/10.1016/j.molcel.2018.09.011, e5.

[30] P. Lu, G. Wang, T. Qian, X. Cai, P. Zhang, M. Li, Y. Shen, C. Xue, H. Wang, The balanced microenvironment regulated by the degradants of appropriate PLGA scaffolds and chitosan conduit promotes peripheral nerve regeneration, Mater. Today Bio 12 (2021), 100158, https://doi.org/10.1016/j.mtbio.2021.100158.

[31] X. Zhou, M. Yu, D. Chen, C. Deng, Q. Zhang, X. Gu, F. Ding, Chitosan nerve grafts incorporated with SKP-SC-EVs induce peripheral nerve regeneration, Tissue Eng. Regen Med. 20 (2023) 309–322, https://doi.org/10.1007/s13770-022-00517-6.

[32] S. Bai, M. Zhang, X. Huang, X. Zhang, C. Lu, J. Song, H. Yang, A bioinspired mineral-organic composite hydrogel as a self-healable and mechanically robust bone graft for promoting bone regeneration, Chem. Eng. J. 413 (2021), 127512, https://doi.org/10.1016/j.cej.2020.127512.

[33] H. Kamata, X. Li, U.-I. Chung, T. Sakai, Design of hydrogels for biomedical applications, Adv. Healthcare Mater. 4 (2015) 2360–2374, https://doi.org/10.1002/adhm.201500076.

[34] K. Rasappan, V. Rajaratnam, Y.-R. Wong, Conduit-based nerve repairs provide greater resistance to tension compared with primary repairs: a biomechanical analysis on large animal samples., plastic and reconstructive surgery, Global Open 6 (2018), https://doi.org/10.1097/GOX.0000000000001981 e1981–e1981.

[35] M. Modrak, M.A.H. Talukder, K. Gurgenashvili, M. Noble, J.C. Elfar, Peripheral nerve injury and myelination: potential therapeutic strategies, J. Neurosci. Res. 98 (2020) 780–795, https://doi.org/10.1002/jnr.24538.

[36] Y. Zhao, Y. Liang, Z. Xu, J. Liu, X. Liu, J. Ma, C. Sun, Y. Yang, Exosomal miR-673-5p from fibroblasts promotes Schwann cell-mediated peripheral neuron myelination by targeting the TSC2/mTORC1/SREBP2 axis, J. Biol. Chem. 298 (2022), 101718, https://doi.org/10.1016/j.jbc.2022.101718.

[37] A.S. Varejão, P. Melo-Pinto, M.F. Meek, V.M. Filipe, J. Bulas-Cruz, Methods for the experimental functional assessment of rat sciatic nerve regeneration, Neurol. Res. 26 (2004) 186–194, https://doi.org/10.1179/016164104225013833.

[38] H. Wang, J. Ma, X. He, Q. Xie, Y. Fu, P. Wang, Investigation for the correlation between brain injury and injured ipsilateral sciatic nerve regeneration in a rat model, JIN 18 (2019) 467–473, https://doi.org/10.31083/j.jin.2019.04.1155.

[39] S.J.P. Pratt, S.B. Shah, C.W. Ward, J.P. Kerr, J.P. Stains, R.M. Lovering, Recovery of altered neuromuscular junction morphology and muscle function in mdx mice after injury, Cell. Mol. Life Sci. 72 (2015) 153–164, https://doi.org/10.1007/s00018-014-1663-7.

[40] Y. Liu, Z. Zhang, Y. Zhang, B. Luo, X. Liu, Y. Cao, R. Pei, Construction of adhesive and bioactive silk fibroin hydrogel for treatment of spinal cord injury, Acta Biomater. 158 (2023) 178–189, https://doi.org/10.1016/j.actbio.2022.12.048.

[41] Q. Min, D.B. Parkinson, X.-P. Dun, Migrating Schwann cells direct axon regeneration within the peripheral nerve bridge, Glia 69 (2021) 235–254, https://doi.org/10.1002/glia.23892.

[42] Z. Yao, W. Yuan, J. Xu, W. Tong, J. Mi, P.-C. Ho, D.H.K. Chow, Y. Li, H. Yao, X. Li, S. Xu, J. Guo, Q. Zhu, L. Bian, L. Qin, Magnesium-encapsulated injectable hydrogel and 3D-engineered polycaprolactone conduit facilitate peripheral nerve regeneration, Adv. Sci. 9 (2022), 2202102, https://doi.org/10.1002/advs.202202102.

[43] X. Dong, S. Liu, Y. Yang, S. Gao, W. Li, J. Cao, Y. Wan, Z. Huang, G. Fan, Q. Chen, H. Wang, M. Zhu, D. Kong, Aligned microfiber-induced macrophage polarization to guide schwann-cell-enabled peripheral nerve regeneration, Biomaterials 272 (2021), 120767, https://doi.org/10.1016/j.biomaterials.2021.120767.